JEAP

ISSN: 2525-815X

Journal of Environmental Analysis and Progress

10.24221/jeap.9.4.2024.7365.356-368

Quantifying filter layer porosity: a comparative study of X-ray microtomography, fluid injection, and fluid saturation techniques

Daiane Francisca do Nascimento Silva[a], Daniel Milian Pérez[a], Yaicel Ge Proenza[a], Bruno Felipe de Carvalho[a], Abel Gámez Rodríguez[a], Antonio Celso Dantas Antonino[a]

[a] Universidade Federal de Pernambuco-UFPE, Departamento de Energia Nuclear. Av. Prof. Luiz Freire, n. 1000, Cidade Universitária, Recife, Pernambuco, Brasil. CEP: 50.740-545. E-mail: daiane.francisca@ufpe.br, daniel.milian@ufpe.br, yaicel.geproenza@ufpe.br, bruno.felipec@ufpe.br, abel.rodriguez@ufpe.br, antonio.antonino@ufpe.br.

ARTICLE INFO

Received 39 Sep 2024
Accepted 04 Dec 2024
Published 16 Dec 2024

ABSTRACT

Wastewater filtration for reuse is a practice applied to conserve water resources. However, its effectiveness is directly related to the permeability of the filter, which can be compromised by clogging processes due to the retention of suspended particles or by precipitated materials while removing chemical contaminants. This study investigated the porous structure of filter layers using different techniques. The study explores porosity in porous media, emphasizing the importance of pores and the interconnected matrix. To evaluate the porosity, fluid injection techniques, fluid saturation techniques, and XR-µCT were employed for porosity determination. It hypothesizes that fluid injection techniques, volumetric measurements, and imaging methods differ in their ability to determine porosity accurately. Nine reference columns of three different porous arrangements were mounted in an acrylic cylinder to study the sensitivity of the techniques to different sizes of matrix arrangements. Finally, the porosity results were compared statistically to determine the error. Fluid injection and saturation techniques are cost-effective methods for determining effective layer porosity. However, experimental studies show that water-based techniques often yield higher porosity than helium gas porosimetry. This discrepancy may be attributed to operational errors inherent to the experimental method, leading to an overestimating porosity. XR-µCT and gas porosimetry are more suitable for quantifying smaller pores. Furthermore, XR-µCT allows for a deeper characterization of the porous medium, such as determining local porosity and applying fluid simulation techniques to observe the permeability and tortuosity of the medium.

Keywords: Porosity characterization, gas porosimeter, volumetric measurements, glass beads, porous media.

Introduction

Considering evident climate change, increasing population, and, consequently, rampant urbanization, the sustainable management of water resources has become a significant challenge (Hu, 2020; Tsekleves et al., 2021). Recent studies highlight the rise in water consumption due to climate change (Muzammil et al., 2023) and the ongoing degradation of water resources due to urban growth (Hu, 2020; Warsame et al., 2023). Water conservation is not only essential when addressed within the scope of public health, but it is also essential in growing food, ensuring food security and human rights (Tsekleves et al., 2021; Wang et al., 2022). The UN 2030 agenda, in its Sustainable Development Goals (SDGs), highlights the importance of this resource conservation, as it addresses issues that directly aim to improve water management and aims to develop knowledge and technologies that can mitigate the effects of climate change and promote the efficient use of water in urban areas. More specifically, this proposal is directly identified with SDG 6, which aims to ensure the availability and sustainable management of water and sanitation for all (Department of Economic and Social Affairs, 2024).

The world's population's continued growth, more stringent quality standards, and increasing drinking water costs have driven efforts to implement water reuse systems. The reuse of different types of water has been a common

practice in water management, with many countries reusing wastewater to address the scarcity of water resources, with guidelines and standards already established. Water treatment technologies, such as reverse osmosis (distillation membranes), which enable seawater desalination and wastewater treatment, are essential for water resource management (Hamdan et al., 2024). Although water reuse in many places is predominantly restricted to sewage treated at treatment plants, it is observed that several industries also reuse wastewater generated in their processes (Noutsopoulos et al., 2018; Hu, 2020; Mahdavi et al., 2020; Tsekleves et al., 2021). In this sense, the retention of contaminants in water is essential in several applications. This includes the prevention and remediation of groundwater contamination using permeable reactive barriers. It is also relevant in industrial applications for the remediation of water contamination after being used in industrial processes. Additionally, the retention of contaminants is crucial for the correction of physical and chemical parameters and for addressing microbiological aspects of reused water intended for both domestic applications and consumption (Song et al., 2021; Sakr et al., 2023; Nguyen et al., 2024; Wyczarska-Kokot et al., 2024). The filtering layers applied for this purpose are composed of inert porous media, capable of removing suspended contaminants, and reactive materials, capable of retaining contaminants dissolved in the fluid (Bai et al., 2024).

Porous media are defined as solid materials containing empty spaces, either interconnected or isolated. The solid portion of the porous medium is referred to as the matrix, while the empty spaces are known as pores. The fundamental characteristics of porous media lie in the presence of pores, which are empty spaces capable of containing various fluids such as water, air, and oils. These pores may be interconnected, allowing for the free permeation of fluids. The analysis of the porous media concept spans various realms of science and engineering, aiming to describe and characterize phenomena and apply these media for particle removal through the filtration method (Song et al., 2023). In the field of soil sciences and hydrology, the soil is meticulously examined as a porous medium capable of retaining and transporting water and nutrients essential for plant growth (Chen et al., 2024), as well as conducting contaminants towards groundwater reservoirs (Dueñas-Moreno et al., 2022; Lee & Jung, 2022; Leal et al., 2023). These processes are governed by the fundamental principles of hydrodynamics and hydrology (Ling et al., 2021).

Every confined space in a porous medium is considered a void region, while the pore region is defined as the volume of the sample that can be filled with fluids. Generally, the larger the pore volume in a sample, the greater the porosity and, consequently, the capacity to store fluids. Porous media are commonly employed to remove particles from fluids, serving as filtering layers. These filtering layers can consist of various materials, such as fibers, meshes, or membranes, and may involve overlapping multiple porous layers. These materials were selected based on the particles' size, shape, and composition characteristics targeted for removal (Zu et al., 2023).

Among the filtering layer applications, Hamisi et al. (2024) investigated sand filter adsorption capacity and treatment efficiency in local treatment systems for cold climate regions. The effects of different operating conditions, porosity, and kinetic parameters were analyzed through column experiments and modeling with COMSOL Multiphysics® (COMSOL, 1998). In sand column experiments, the results indicated that the total phosphorus adsorption rate depended on the feed water quality. Adsorption in the septic tank effluent was highest, followed by the biotreatment effluent and the Polonite® reactive material. The results demonstrated that treating local wastewater in cold weather with tidal flow constructed wetland (TFCW) can effectively treat effluent from a three-step pretreatment system. However, hydraulic optimization is crucial in ensuring long-term system operation success.

Despite the benefits of the filtration process, the water used to maintain the filters (backwash water) is a major concern. To investigate possible ways to remedy this problem, Mahdavi et al. (2024) managed to get this backwash water to reach acceptable parameters for consumption through the ultrafiltration process in a chemical reactor.

In the filtration process, particles are retained in the pores of the layer by retention mechanisms so that the porous structure evolves based on the patterns of this retention (Deng et al., 2022; Civan, 2023; Elrahmani et al., 2023). When the pores of the filter layers are clogged, the flow is restricted, as the clogging of the pores creates a barrier that makes it difficult for water to pass through the filter. As the obstruction increases, the space available for flow decreases, resulting in reduced water flow. Another consequence of clogging is the increase in differential pressure since the water needs to exert greater pressure to overcome the obstruction and pass through the filter. This leads to an increase in the differential pressure between the inlet and outlet. In general,

reducing the porosity of filtering layers results in the loss of filtration efficiency in its physical and, consequently, chemical aspects (Hariti et al., 2019; Civan, 2023; Monga et al., 2023).

The appropriate choice of the filtering layer is crucial to ensure that the fluid is effectively purified or treated without adversely affecting its chemical and physical properties. Thus, it is essential to analyze the porosity, permeability, and, if possible, the tortuosity of filter layers before their practical application (Berry et al., 2023; Li et al., 2023). Among the experimental methods employed in porosimetry of porous media, notable techniques, including volumetric measurements and imaging techniques such as X-ray Computed Microtomography (XR-μCT), are applied.

Volumetric porosimetry techniques based on materialized volume measurements involve determining the volumes of pores and porous matrices measured from the volume occupied by injected/infiltrated fluids in the samples. A limiting factor for these techniques is the inability to determine the volume of isolated pores since only the volume of pores accessed by the fluid is measured, also known as the effective porosity of the medium (interconnected pores) (Silva et al., 2023). However, imaging porosimetry techniques, such as XR-μCT, allow for the visualization of both connected and isolated pores within a sample, providing high precision in determining the absolute porosity of the medium (Haide et al., 2022). So, in general, porosimetry by XR-μCT includes precise information about the geometry, size, distribution, and connectivity of the pores present in the sample (Liu et al., 2023). Despite the variety of techniques available for characterizing porous media, applying the technique that best suits the specific characteristics of the sample set under study is crucial to ensuring the high efficiency of these layers.

Another decisive factor for selecting a filtering layer is permeability, which is the ability of the porous medium to allow the movement of fluids through it and is directly related to its velocity. It is affected by pores' size, shape, distribution, and interconnectivity. In more concise terms, a porous medium with a large volume of pores distributed evenly throughout the sample, assuming all pores are interconnected, allows fluids to pass through it with less resistance. Other factors, such as the distribution of pore sizes and the tortuosity of the porous medium, can influence permeability. Tortuosity measures the curvature of fluids' paths within the porous medium. It is directly related to the pores' shape and spatial distribution. As a rule, it affects the resistance to fluid flow within the porous medium. The greater the tortuosity, the more sinuous the paths followed by the fluids, and the greater the resistance to flow (Costa, 2006; Cai et al., 2019; Conzelmann et al., 2022). The tortuosity of porous media is closely linked to permeability, which is related to porosity. However, although these links are noted, there is no explicit understanding of the synergistic effect of tortuosity on permeability. However, it is known that the greater the tortuosity of the medium, the more difficult it will be for a fluid to percolate through it. In general, we can assume that the more difficult it is for a particle to be percolated in this fluid, the greater the incidence of elastic collisions will be, which will cause a decrease in its velocity and consequent retention in the medium due to the various particle retention mechanisms in the pores (Sacramento et al., 2015; Sadeghnejad et al., 2022; Civan, 2023; Monga et al., 2023).

In a brief bibliographic overview, the literature shows that in liquid intrusion porosimetry, mercury is commonly used for hydrophilic porous media and water for hydrophobic porous media (Giesche, 2006; Rouquerol et al., 2012). Water intrusion into hydrophobic media has been widely studied to attest to its efficiency and advantages over other porosimetry methods (Rouquerol et al., 2012; Kuila et al., 2014; Jarrahi et al., 2019). In this sense, tests to determine the porosity of shale carried out by Kuila et al. (2014) demonstrated the high reproducibility and effectiveness of the Water Immersion Porosimetry (WIP) method about the Mercury Intrusion Porosimetry (MIP) method, finding that mercury could not fully access the shale pore structure. In agreement, Jarrahi et al. (2019), when determining the porosity of concrete samples using the MIP, NMR, Gas Expansion (GE), and Gas Expansion Induced from Water Intrusion Porosimetry (GEIWIP) techniques, they found that GEIWIP proved to be as effective as the others. However, GEIWIP presented a better cost-benefit ratio than nuclear magnetic resonance and a shorter sample preparation time than MIP. Considering the complementary nature of volumetric measurements with water and helium gas in characterizing porous materials, the following techniques were used in this work: helium gas porosimetry, as an injection technique, and gravimetry, both direct and indirect porosimetry, as saturation techniques.

Given the importance of selecting suitable porous media components for constructing a filtering layer and choosing the most effective characterization technique, this study aimed to characterize different porous media to be used as analogs for filtering layers, illustrating the pore distribution throughout the samples. The main

objective of this is to study the porosity of porous media analogous to filter layers using the fluid injection technique (helium gas porosimetry), fluid saturation (direct porosimetry and gravimetry), measurements of materialized volumes (indirect porosimetry), and XR-μCT.

Material and Methods

This study used nine filtering layers, called reference columns, assembled in an acrylic cylinder using glass beads as a solid matrix. Considering the nine filtering layers constructed, three were composed of 3 mm diameter glass beads (CF3), 3 were 4 mm (CF4), and another three were composed of 4- and 3-mm beads mixed in a proportion of ½ each (CFM). The samples' porosity was determined using the previously described techniques, and the averages of the sets (average porosity of the triplicates) were analyzed. Table 1 presents the cylinders' dimensions used for samples.

Table 1. Dimensions (mm) of the acrylic cylinders of the reference columns. Font: Silva et al. (2024).

Column group	Sample	Length	Internal diameter	External diameter
CF3	1	49.76	25.55	31.54
	2	49.91	26.36	31.58
	3	49.64	25.76	31.46
CF4	1	49.81	25.63	31.66
	2	49.71	25.56	31.59
	3	49.86	25.61	31.57
CFM	1	49.94	26.16	31.80
	2	49.79	25.43	31.53
	3	49.87	25.42	31.52

Using glass beads in the reference columns was essential at this stage. Their regular surface ensures that, as they have well-defined and connected voids, the medium presents absolute porosity equal to the effective porosity (important for porosimetry methods based on column saturation). Despite efforts to obtain a medium with constant and homogeneous porosity, the beads did not present a perfectly spherical shape. Ellipsoids were easily visualized within the same diameter set, as shown in Figure 1. This variability in pebble shape led to variations in their arrangement within a column containing the same quantity per unit. This suggests that rearrangement could result in media with small porosity variations when assembling and disassembling a column while maintaining component integrity. Therefore, it is necessary to highlight this fact, as the samples needed to be disassembled to dry the beads after applying each water saturation-based porosimetry method and reassembled for subsequent methods.

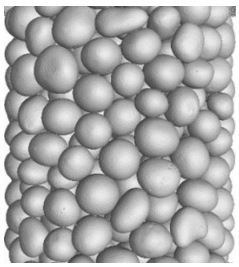

Figure 1. Shapes variation of glass beads. Font: Silva et al. (2024).

This study used three porous arrangements that differed in the size of the matrix particles. The variation in the average diameters of the glass beads was necessary to evaluate the sensitivity of the methods to porosity variations, as larger particles in the porous matrix of filter layers result in a larger void volume. Therefore, samples composed of 4 mm beads are generally expected to exhibit higher porosity than those of 3 mm beads. expected. An intermediate porosity is expected for samples of a mixture of both diameters, as smaller particles are expected to fill the spaces between the larger particles, reducing the void volume. However, since the beads' diameters are similar, a large difference between these porosities is not anticipated.

After porosity measurements, the data obtained by each technique were compared to identify congruencies and/or inconsistencies of all methods applied. Subsequently, the porosity of these layers was determined using the fluid injection porosimetry methods. Finally, the porosities determined by the different methods were compared and discussed to highlight factors capable of causing inconsistencies in data obtained by the X-ray computed tomography technique.

Techniques of porosity determination: Fluid injection and fluid saturation techniques

One of the most common ways to determine a medium's porosity is to fill its pores with a fluid, such as liquids (liquid intrusion

porosimetry or liquid immersion porosimetry) or gases (gas porosimetry/gas expansion). In this way, the volume of fluid necessary to fill the sample pores is adopted as the volume of interconnected pores (Rouquerol et al., 2012; Labani et al., 2013; Kuila et al., 2014; Silva et al., 2023).

The functionality principle of the helium gas porosimeter is based on the ideal gas law, which describes the behavior of gases in terms of volume, pressure, temperature, and quantity of substance. According to this law, the pressure of a gas is inversely proportional to the volume it occupies if the temperature and quantity of substance are kept constant. This relationship is also known as Boyle's law. The sample is placed in an evacuated chamber, and the pores introduce and absorb helium gas. The helium pressure in the chamber is monitored, and the data is used to calculate the amount of helium absorbed. Figure 2 illustrates the organizational scheme arranged in conventional helium gas porosimeter equipment. The helium gas porosimeter DCI Test System was used. As it is a porous layer inside an acrylic cylinder, it was necessary to consider the volume of the cylinder wall as a spacer for the equipment itself to minimize its influence on the porosity of the sample.

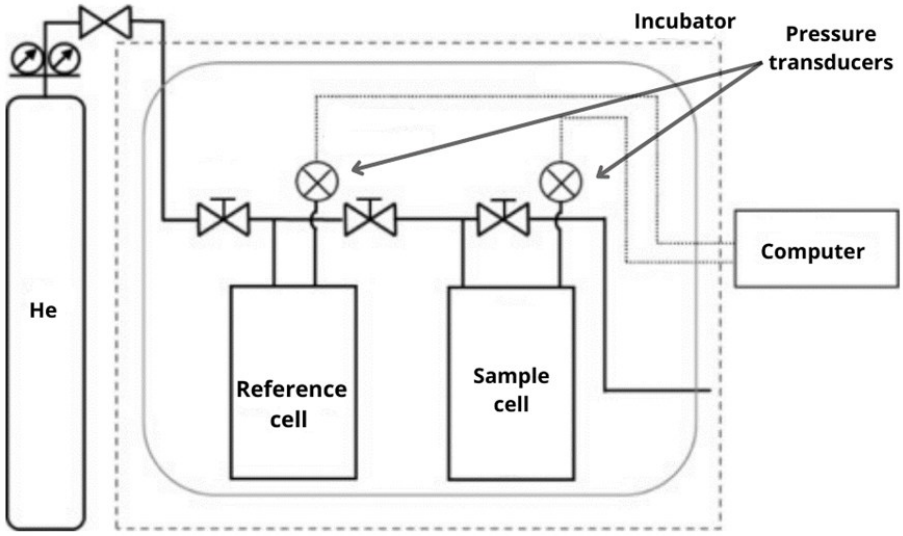

Figure 2. Schematic diagram of a helium gas porosimeter. Font: Sun et al. (2016).

Considering fluid saturation porosimetry methods, distilled water was used as pore-filling fluid since damage was observed in acrylic cylinders exposed to alcohol in preliminary tests where absolute ethyl alcohol PA (99.95%) was used.

The gravimetric method relies on measuring the increase in mass of a liquid filling the sample's pores. The procedure begins with weighing the dry sample using an analytical balance model BL3200H (Shimadzu), designated as mass 1, using an analytical balance. Subsequently, the pores are filled with distilled water, and the sample is immersed long enough for the liquid to penetrate the pores, avoiding air retention fully. The mass of the sample plus the liquid is measured and referred to as mass 2. The liquid mass is calculated as the difference between masses 1 and 2, so the liquid volume is determined based on the liquid mass and density. Finally, porosity is determined from the ratio of the water-filled volume to the total volume of the acrylic cylinder.

The porosimetry or direct porosimetry method determines the volume of voids in a porous sample based on the volume occupied by a liquid that fills the material's pores. It is a considerably simple and easy-to-perform method that requires only a burette and liquid. The procedure began with one end of the columns' acrylic cylinders being sealed with plastic film to retain the liquid in the cylinder. A PVC disc was also used under the base of the connector to support the sealed end and prevent plastic deformation due to the weight of the liquid. With the sample dry and the 50 mL buret duly filled, it began to be filled with liquid cautiously, avoiding the air retention in the liquid. The volume of liquid indicated by the burette refers to the pore volume of the sample.

This technique determines porosity based on the volume occupied by the sample solids, to determine the porosity. The glass beads that compose the porous media were transferred to

volumetric flasks. The volumetric flask was filled with distilled water up to the mark indicated by the glassware. The difference between the volume of the volumetric flask and the volume of water used, as noted in the burette, results in the volume of the glass bead cluster. The difference between the empty acrylic cylinder's volume and the glass beads' volume determines the total pore volume.

Techniques of porosity determination: X-ray Computed Microtomography

Computed tomography (CT) is an advanced imaging technique with a wide range of applications in different fields, including materials science. When applied as a non-destructive method, CT plays a fundamental role in characterizing materials and structures, such as determining porosity (Rouquerol et al., 2012; Haide et al., 2022; Silva et al., 2023). CT is based on capturing two-dimensional images of cross-sections of an object and computationally reconstructing these sections into a three-dimensional image. In the case of XR-μCT, X-rays are used and produced in the microtomography device. Porosity via X-ray Computed Tomography is based on the attenuation suffered by X-ray beams falling on a sample between the source and the detector, as shown in Figure 3. These attenuation variations are captured by sensors, converted into output signals, and transformed into digital images. The resulting projections represent the distribution of the material throughout the sample.

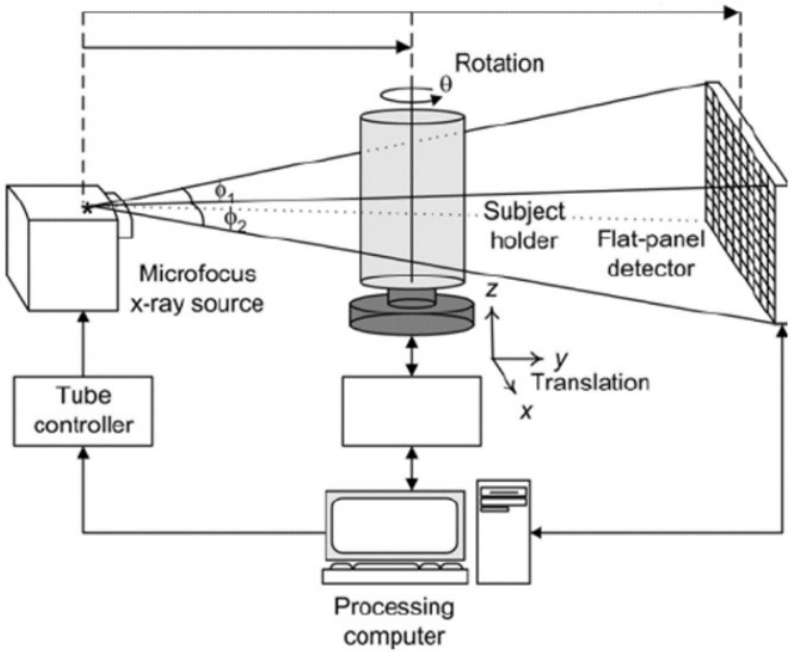

Figure 3. Schematic representation of scanning samples on an x-ray microtomography. Font: Lüthi et al. (2003).

The tomographic images of the studied samples were obtained with a third generation XR-μCT device model NIKON XT H 225 ST, located at LTC-RX - DEN/UFPE. The following scanning conditions were used: voltage of 200 kV, current equal to 90 μA, Copper (Cu) filter of 0.5 mm, and resolution of 25 μm. The tomographic projections were reconstructed using the CTPro 3D XT 3.03 (Nikon Metrology, 2015), where the projections are pre-processed to correct noise, artifacts, and imperfections so that in the reconstruction process, the reconstruction algorithms (x for symmetric data sets and y for asymmetric data sets) calculate the attenuation values in each three-dimensional voxel of the image. Once generated, the sample volume to be studied was selected and cut to eliminate the wall of the acrylic tube (Nikon Metrology, 2015). After selecting the volume of interest, the samples were processed and segmented using the VGStudio Max 3.4.4 (Volume Graphics, 2020). In the processing stage, the Gaussian filter was applied to all samples to eliminate noise artifacts on the surface of the beads. Considering the porosity calculation, it was necessary to segment the sample (a process in which the image is separated into regions, in this case, voids and non-voids).

Afterward, porosity was calculated by the relationship between the total volume of the sample and the volume of pores identified in the software's segmentation process. Initial analyses showed the non-uniformity of the internal volume of acrylic cylinders. Therefore, for segmentations, the sample volume was divided into seven subvolumes of the same dimensions (280 voxels) (shown in Figure

4e) to encompass most of the sample in the porosity calculation without suffering interference from the wall of the acrylic cylinder. In addition to determining the porosity of the samples, the software VGStudio Max 3.4.4 (Volume Graphics, 2020) also allows the characterization of permeability and tortuosity over the entire sample length.

Another advantage of applying the technique of XR-µCT is that it allows the characterization of the medium in terms of its flow properties, such as permeability and tortuosity. Therefore, after calculating the porosity of the samples for every arrangement, a single column was subjected to simultaneous porosity and permeability tests. Considering the tortuosity and permeability analyses, the volume generated by CTPro 3D XT 3.03 (Nikon Metrology, 2015) previously acquired from XR-µCT was used. A new total volume is thus selected, unifying the previously selected subvolumes to determine porosity in the VGStudio Max 3.4.4 (Volume Graphics, 2020) considering water as a percolating fluid, setting a velocity of $5.13e^{-6}$ $m^3.s^{-1}$ (injection of 10 $mm.s^{-1}$). Hydraulic tortuosity was calculated from the ratio between the average velocity of a fluid in a reference medium (without flow resistance) of the same dimensions as the segmented one (u) and the average velocity of the fluid in the studied porous medium (u_n), both in same gradient conditions. Consequently, a tortuosity value closer to one indicates higher flow velocity and lower resistance.

Figure 4 shows the samples studied (Figure 4a), the equipment used to scan the samples (Figure 4b), the projections obtained (Figure 4c), the view of the volume with the projections overlapping (Figure 4d), the subvolumes sectioned in the samples to calculate porosity (Figure 4e), and the representation of the volume used to simulate the permeability and calculate the tortuosity analysis (Figure 4f). The axial velocity was calculated using the axes' direction, as shown in Figure 5.

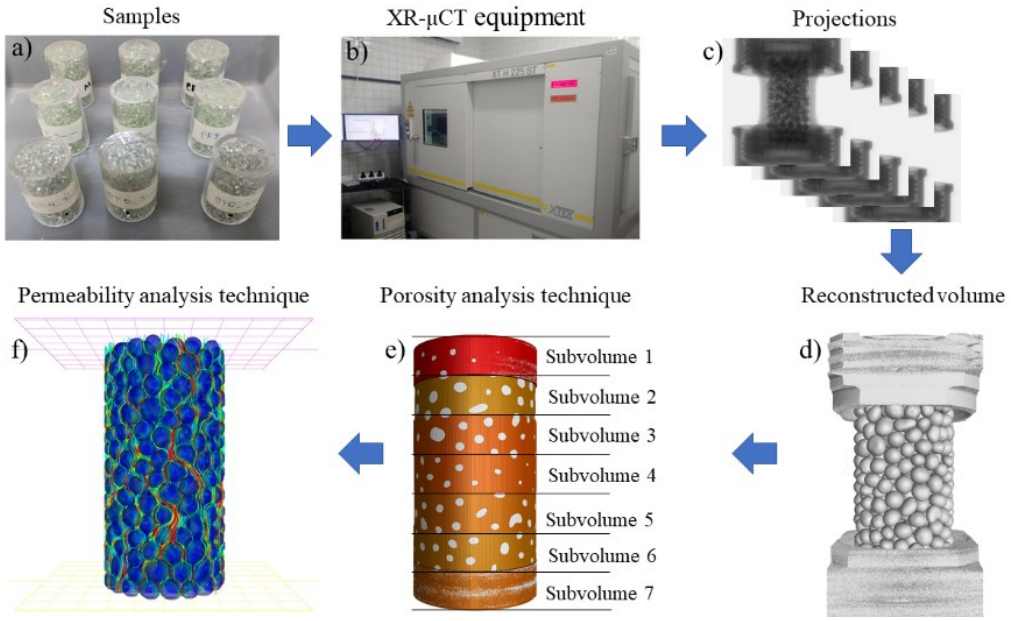

Figure 4. Methodology for determining the porosity, tortuosity, and permeability of filtering layers using the XR-µCT technique. Font: Silva et al. (2024).

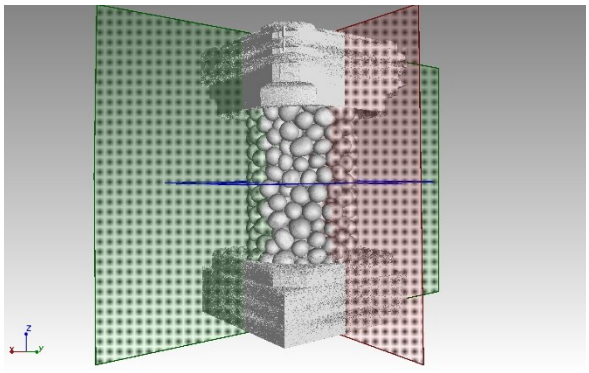

Figure 5. Direction of the axes of the columns. Font: Silva et al. (2024).

Results and Discussion

Porosity analysis

Table 2 presents the results of the porosity (%) measurements in three types of column arrangements (CF3, CF4, and CFM) using five different techniques: direct porosimetry, gravimetry, indirect porosimetry, gas porosimetry and X-ray computer micro-tomography (XR-µCT. Three replicas were measured for each combination of technique and column. The average value and associated standard error € were reported.

Table 2. Porosity (%) measurements using different techniques. Font: Silva et al. (2024).

Column type	Sample	Direct porosimetry	Gravimetry	Indirect porosimetry	Gas porosimetry	XR-µCT
CF3	1	38.70	38.07	39.05	37.14	35.95
	2	40.07	40.10	38.95	38.93	36.86
	3	41.00	40.95	40.10	39.86	37.99
	Mean*	39.92 ± 0.67	39.71 ± 0.85	39.37 ± 0.37	38.64 ± 0.80	36.93 ± 0.59
CF4	1	40.70	40.33	40.87	39.51	38.62
	2	40.86	40.94	41.20	40.12	38.64
	3	40.15	40.48	40.04	39.17	38.04
	Mean*	40.57 ± 0.22	40.58 ± 0.18	40.70 ± 0.35	39.60 ± 0.28	38.43 ± 0.20
CFM	1	40.00	39.96	38.92	37.55	36.51
	2	40.00	40.25	39.11	36.67	36.07
	3	40.15	40.07	38.01	36.83	36.44
	Mean*	40.05 ± 0.05	40.09 ± 0.08	38.68 ± 0.34	37.02 ± 0.27	36.34 ± 0.14

* The reported value is the confidence interval at 95% for the mean: $\bar{x} \pm e$.

The mean relative errors (calculated as the average of $100e/\bar{x}$) of the porosity measurements are within 2.5% for all techniques, which reflects the good precision of the determinations. These data allow valuable insights into the accuracy and dispersion of the different porosity measurement techniques for the CF3, CF4, and CFM column types. For instance, direct porosimetry is the most accurate technique, displaying the lowest average relative error (0.78%), especially for the CFM column arrangements, for which the mean entails a standard error of only 0.05%. In contrast, gas porosimetry seems the least accurate, with a higher mean relative error of 1.17% (from standard errors, 0.80%, 0.28%, and 0.27% for CF3, CF4, and CFM, respectively).

Regarding dispersion, Figure 6 shows the mean porosity values (%) with standard error bars (data with star symbols in Table 2) for all used techniques, grouped by the different column types.

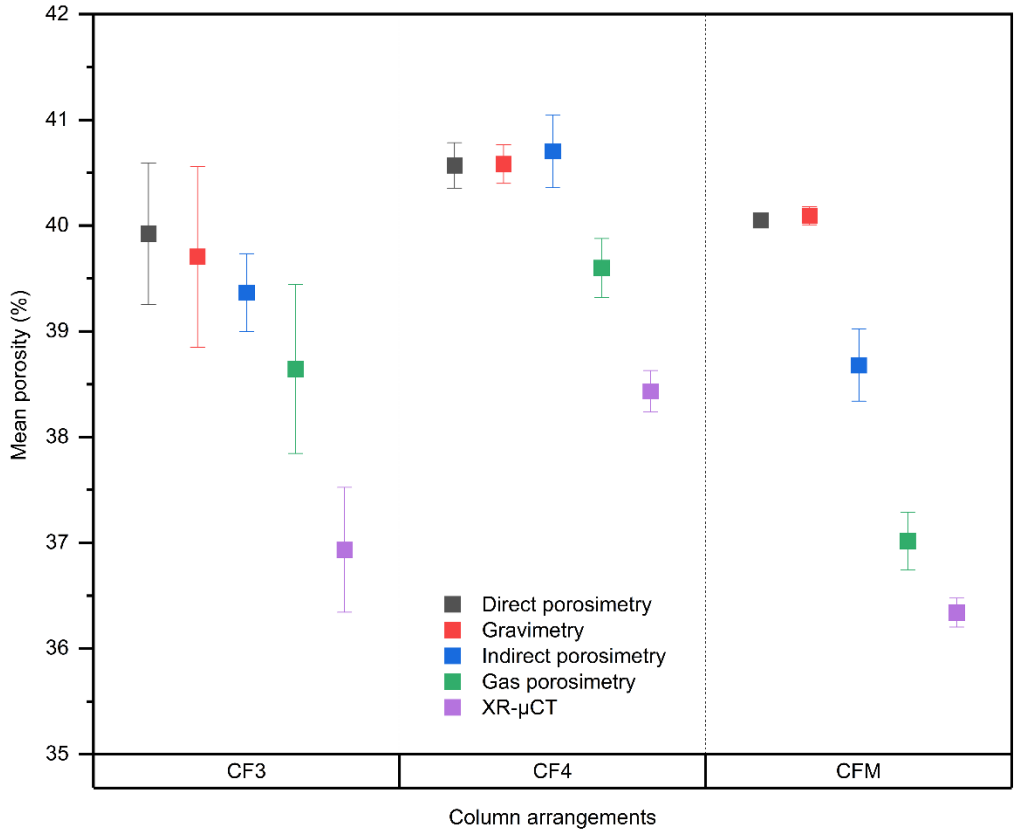

Figure 6. Mean porosity (%) from replicated measurements grouped by column type. Font: Silva et al. (2024).

The direct porosimetry and gravimetry techniques (grey and red squares in Figure 6, respectively) yield higher porosity values across all columns, with no significant differences at a 95%

confidence level. The mean porosity from these two methods appears consistent, particularly in the CF3 and CFM columns, while a noticeable drop was observed for the CF4 columns. The porosity values determined through indirect porosimetry (blue squares in Figure 6) are not statistically different (5% significance level) from the porosity values determined with direct porosimetry or gravimetry for the CF3 and CF4 columns (beads with 3 mm and 4 mm of diameter, respectively), but a significant decrease was observed in the mean porosity value for CFM columns (with equal quantities of 3 mm and 4 mm beads). This suggests indirect porosimetry could be more sensitive to particle size variations than the former two techniques.

The gas porosimetry and XR-μCT techniques (green and purple squares in Figure 6, respectively) show larger variations in the measured porosity values across column types, with the highest values for the CF4 column and the lowest for the CFM columns. The noticeable drop in the porosity values measured with these two methods when moving from CF4 to CF3 and CFM is statistically significant at the 0.05 level, which highlights the capability of gas porosimetry and XR-μCT to capture finer structural details that might contribute to lower porosity readings.

When observing the porosity determinations using different methods within column arrangements, it is noticeable that the broadest range of porosity values across techniques is from 36.34 ± 0.14 to 40.70 ± 0.35. The mean porosity values in the CF4 column are higher than their respective values in CF3 and CFM, and no relevant differences were observed between the last two. Direct porosimetry and gravimetry yield the highest porosity values regardless of the diameters of the confined beads (they are on the top of the three columns in Figure 6), while XR-μCT provides the lowest porosities.

Besides the mean porosity values, it is important to observe the error bars in Figure 6, which suggest the variability of the measurements for each technique/column pair, where longer bars indicate greater variability and shorter bars indicate more consistent measurements. For instance, the greatest dispersion was observed while measuring the porosity in CF3 columns no matter the technique, from ± ±0.37 to ± 0.85, and the smallest dispersion was observed in the CFM columns with a minimal standard error of ± 0.05 (Table 2). This suggests that obtaining porosity measurements in materials with small particle sizes (low pebble diameters) is less accurate than in materials with high porosity or mixed particle sizes. Noteworthy, this should be correlated to a higher organizational space with small beads, with larger variations in bead positioning during column preparation, resulting in a wider range for porosity. In contrast, the conformational space is restricted for CFM and CF4 columns with larger particle sizes, and little fluctuation in the porosity measurements should be observed.

A two-way repeated measures ANOVA was performed with data to have a thorough statistical criterium for this study. Mauchly's test of sphericity showed $W = 0$ and p-value < 0.0001 for technique and technique/column interactions, which means that the variances of the differences between all pairing combinations are not equal, violating the fundamental assumption of sphericity for repeated measures ANOVA. Therefore, the Greenhouse-Geisser correction was used for comparisons involving the technique factor. Regarding the column factor, the assumption of sphericity was met with Mauchly's $W = 0.18033$ and p-value = 0.4247.

Considering these criteria, the test of within-factors effects of the ANOVA indicates a highly significant effect of the technique on porosity, with $F \approx 73.86$ and p-value = 0.0045 < 0.05 considering the Greenhouse-Geisser correction. This suggests that different measurement techniques (at least one of the studied techniques) lead to statistically significant differences in porosity measurements. Conversely, both statistics $F \approx 3.23$ with p-value = 0.15 > 0.05 (sphericity assumed) for a column, and $F \approx 8.55$ with p-value = 0.07 > 0.05 (Greenhouse-Geisser correction) for technique/column interaction, respectively, indicate that porosity does not differ significantly between the columns (CF3, CF4, and CFM), at the 0.05 level. Furthermore, the test of between-factors effects of the ANOVA shows off a highly significant intercept ($F \approx 60441$, $p < 0.0001$) with a very small error (mean square = 1.1388). This reflects the overall mean porosity across all analyzed factors and confirms that the mean porosity of the samples is significantly different from zero (due to the interception) and that the observed differences are primarily due to the within-factors effects (mainly technique) rather than individual differences between columns.

The pairwise comparisons by technique and column types, according to the grouping letters tables of the ANOVA, are represented in Figure 7. Note that the variation in porosity between techniques is larger than between column types. Regarding the technique, the porosity measurements using direct porosimetry, gravimetry, and indirect porosimetry are statistically equivalent (the three circles at the top-

left of Figure 7 intercept each other) at the 0.05 significance level, yielding higher porosity values as compared to gas porosimetry, and even higher than XR-µCT technique, which systematically returns the lowest porosity for all particle sizes in the columns. Relating the column type, the highest mean porosity was obtained for the CF4 column, containing the 4 mm of diameter beads, and this porosity is statistically different from the two mean values obtained on CF3 and CFM columns, which show non-statistical differences between each other (bottom-right circles in Figure 7 superpose).

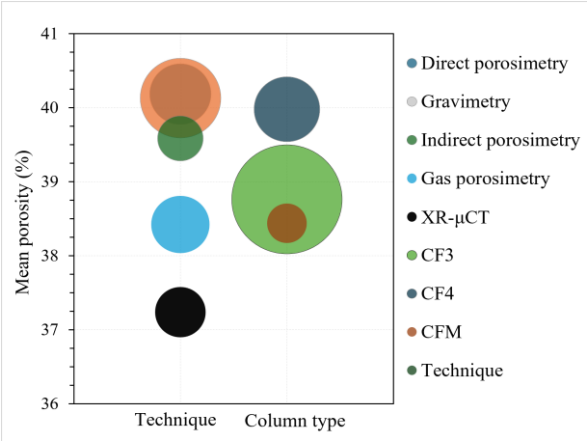

Figure 7. Mean porosity (%) considering all measurements grouped by Technique and Column type. The pebble diameters are two times the standard error of the mean, representing the actual 95% confidence intervals. Font: Silva et al. (2024).

Tortuosity and permeability analysis

Characterizing the fluid medium of each arrangement using the XR-µCT technique presented tortuosity values of 1.26 for CF3, 1.30 for CF4, and 1.27 for CFM, revealing that the porous media studied possess low resistance properties. The permeability observed in these columns was 7.21 x 10^{-9} m², 1.07 x 10^{-8} m² and 8.92 x 10^{-9} m², respectively. These data show greater tortuosity of the column representing the CF4 arrangement. The data suggests that column CF4, despite exhibiting higher permeability than columns CF3 and CFM, also presents higher flow resistance due to its elevated tortuosity. This characteristic can be attributed to the unique arrangement of column CF4, composed of just 4 mm beads, resulting in larger pores. However, the large particle size in the porous matrix of column CF4 leads to more tortuous channels (complex porous structure), increasing flow resistance.

A review of the literature revealed that Silvia et al. (2012) reported permeabilities ranging from 1.65 x 10^{-16} m² to 3.16 x 10^{-15} m² for ceramic filters produced via sol-gel methods, and 1.38 x 10^{-16} m² to 8.72 x 10^{-13} m² for simple mixtures with polyethylene glycol. Despite comparable porosities, the permeability values obtained in our study were higher than those reported by Silvia et al. (2012), suggesting that material composition and production techniques significantly influence flow resistance and permeability in porous media. This comparison underscores the critical role of particle size and arrangement in determining the hydraulic properties of filter layers. Nonetheless, the efficiency of these media cannot be determined solely by these parameters, given that permeability fluctuates according to the specific application, such as the size of particles to be filtered.

Conclusion

XR-µCT consistently yields lower porosity values due to its higher resolution, while other techniques demonstrate varying sensitivity to different column types. Statistical corrections are crucial for accurate porosity analysis.

Fluid injection and saturation techniques offer cost-effective porosity determination of filter layers. However, experimental studies reveal that water-based techniques (direct, indirect porosimetry, and gravimetry) may overestimate porosity compared to helium gas porosimetry. The sample measurement process makes gas porosimetry less susceptible to such errors. All techniques yielded consistent porosities within the CF4 and CFM sets.

The main observation indicates that all techniques can estimate filter layer porosity, making fluid injection and saturation more affordable. XR-µCT offers a distinct advantage by enabling local tortuosity value determination and permeability simulation. The choice of filter layer depends on the specific application. For applications that require high permeability and retention, CF4 may be optimal, while CF3 might be more suitable for high particle retention. Overall, this study demonstrated the potential of XR-µCT for optimizing filter layer design by balancing permeability and particle retention.

Acknowledgments

This research was partially supported by the Fundação de Amparo à Ciência e Tecnologia de Pernambuco (FACEPE), project numbers: IBPG-1064-3.09/22 and BFP-0146-3.09/23 and the Conselho Nacional de Desenvolvimento Científico e Tecnológico (CNPq), project number: 465764/2014-2 Observatório Nacional da Dinâmica da Água e de Carbono no Bioma Caatinga (ONDACBC). The authors also acknowledge CNPq for research support, including the Junior Postdoctoral Fellowship awarded to

Abel Gámez Rodríguez (Process number 174032/2023-4) and the Productivity Fellowship granted to Antonio Celso Dantas Antonino.

References

Bai, X.; Samari-Kermani, M.; Schijven, J.; Raoof, A.; Dinkla, I. J. T.; Muyzer, G. 2024. Enhancing slow sand filtration for safe drinking water production: interdisciplinary insights into Schmutzdecke characteristics and filtration performance in mini-scale filters. Water Research, 262, (2024), 122059. https://doi.org/10.1016/j.watres.2024.122059

Berry, G.; Beckman, I.; Cho, H. 2023. A comprehensive review of particle loading models of fibrous air filters. Journal of Aerosol Science, 167, (2023), 106078. https://doi.org/10.1016/j.jaerosci.2022.106078

Cai, J.; Zhang, Z.; Wei, W.; Guo, D.; Li, S.; Zhao, P. 2019. The critical factors for permeability-formation factor relation in reservoir rocks: Pore-throat ratio, tortuosity and connectivity. Energy, 188, (2019), 116051. https://doi.org/10.1016/j.energy.2019.116051

Chen, X.; Yu, Z.; Yi, P.; Hwang, H. T.; Sudicky, E. A.; Tang, T.; Aldahan, A. 2024. Effects of soil heterogeneity and preferential flow on the water flow and isotope transport in an experimental hillslope. Science of the Total Environment, 917, (2024), 170548. https://doi.org/10.1016/j.scitotenv.2024.170548

Civan, F. 2023. Multiphase and multispecies transport in porous media. Reservoir Formation Damage, 4, 257-273. https://doi.org/10.1016/B978-0-323-90228-1.00026-1

COMSOL. Multiphysics Reference Manual. 1998. [Online WWW]. Available at: www.comsol.com/blogs. Access at: October 30, 2024.

Conzelmann, N. A.; Partl, M. N.; Clemens, F. J.; Müller, C. R.; Poulikakos, L. D. 2022. Effect of artificial aggregate shapes on the porosity, tortuosity and permeability of their packings. Powder Technology, 397, (2022), 117019. https://doi.org/10.1016/j.powtec.2021.11.063

Costa, A. 2006. Permeability-porosity relationship: A reexamination of the Kozeny-Carman equation based on a fractal pore-space geometry assumption. Geophysical Research Letters, 33, (2006), L02318. https://doi.org/10.1029/2005GL025134

Deng, H.; Gharasoo, M.; Zhang, L.; Dai, Z.; Hajizadeh, A.; Peters, C. A.; Soulaine, C.; Thullner, M.; Van Cappellen, P. 2022. A perspective on applied geochemistry in porous media: Reactive transport modeling of geochemical dynamics and the interplay with flow phenomena and physical alteration. Applied Geochemistry, 146, (2022), 105445. https://doi.org/10.1016/j.apgeochem.2022.105445

Department of Economic and Social Affairs. 2024. Sustainable Development. United Nations. [Online WWW]. Available at: https://sdgs.un.org. Access at: October 30, 2024

Dueñas-Moreno, J.; Mora, A.; Cervantes-Avilés, P.; Mahlknecht, J. 2022. Groundwater contamination pathways of phthalates and bisphenol A: origin, characteristics, transport, and fate – A review. Environment International, 170, (2022), 107550. https://doi.org/10.1016/j.envint.2022.107550

Elrahmani, A.; Al-Raoush, R. I.; Seers, T. D. 2023. Clogging and permeability reduction dynamics in porous media: A numerical simulation study. Powder Technology, 427, (2023), 118736. https://doi.org/10.1016/j.powtec.2023.118736

Giesche, H. 2006. Mercury Porosimetry: A General (Practical) Overview. Particle & Particle Systems Characterization, 23, 9-19.

Haide, R.; Fest-Santini, S.; Santini, M. 2022. Use of X-ray micro-computed tomography for the investigation of drying processes in porous media: A review. Drying Technology, 40, 1731-1744. https://doi.org/10.1080/07373937.2021.1876723

Hamdan, S.; Al-Ghafri, B.; Al-Obaidani, S.; Tarboush, B. A.; Al-Sabahi, J.; Al-Abri, M. 2024. Dairy wastewater treatment with direct-contact membrane distillation in Oman. Desalination and Water Treatment, 320, (2024), 100672. https://doi.org/10.1016/j.dwt.2024.100672

Hamisi, R.; Renman, A.; Renman, G.; Wörman, A.; Thunvik, R. 2024. Treatment efficiency and recovery in sand filters for on-site wastewater treatment: Column studies and reactive modelling. Journal of Cleaner Production, 462, (2024), 142696. https://doi.org/10.1016/j.jclepro.2024.142696

Hariti, Y.; Hajji, Y.; Hader, A.; Faraji, H.; Boughaleb, Y.; Faraji, M.; Saifaoui, D. 2019. Modelling of fluid flow in porous media and filtering water process: Langevin dynamics and Darcy's law based approach. Materials

Today: Proceedings, 30, 870-875. https://doi.org/10.1016/j.matpr.2020.04.343

Hu, R. 2020. Pollution control and remediation of rural water resource based on urbanization perspective. Environmental Technology and Innovation, 20, (2020), 101136. https://doi.org/10.1016/j.eti.2020.101136

Jarrahi, M.; Ruth, D. W.; Bassuoni, M. T.; Holländer, H. M. 2019. Porosity Measurement of Low Permeable Materials Using Gas Expansion Induced Water Intrusion Porosimetry (GEIWIP). Scientific Reports, 9, (2019), 17554. https://doi.org/10.1038/s41598-019-53441-6

Kuila, U.; McCarty, D. K.; Derkowski, A.; Fischer, T. B.; Prasad, M. 2014. Total porosity measurement in gas shales by the water immersion porosimetry (WIP) method. Fuel, 117, 1115-1129. https://doi.org/10.1016/j.fuel.2013.09.073

Labani, M. M.; Rezaee, R.; Saeedi, A.; Hinai, A. Al. 2013. Evaluation of pore size spectrum of gas shale reservoirs using low pressure nitrogen adsorption, gas expansion and mercury porosimetry: A case study from the Perth and Canning Basins, Western Australia. Journal of Petroleum Science and Engineering, 112, 7-16. https://doi.org/10.1016/j.petrol.2013.11.022

Leal, J.; Avila, E. A.; Darghan, A. E.; Lobo, D. 2023. Spatial modeling of infiltration and its relationship with surface coverage of rock fragments and porosity in soils of an Andean micro-watershed in Tolima (Colombia). Geoderma Regional, 33, (2023), e00637. https://doi.org/10.1016/j.geodrs.2023.e00637

Lee, J.; Jung, H. 2022. Understanding the relationship between meltwater discharge and solute concentration by modeling solute transport in a snowpack in snow-dominated regions – A review. Polar Science, 31, (2022), 100782. https://doi.org/10.1016/j.polar.2021.100782

Li, L.; Zhou, Y.; Sun, Z.; Gu, H.; Shi, J.; Wang, X.; Chen, M.; Zhao, Z. 2023. Improved design of metal fiber filter materials: Experiment and theory. Journal of Membrane Science, 675, (2023), 121559. https://doi.org/10.1016/j.memsci.2023.121559

Ling, X.; Yan, Z.; Liu, Y.; Lu, G. 2021. Transport of nanoparticles in porous media and its effects on the co-existing pollutants. Environmental Pollution, 283, (2021), 117098. https://doi.org/10.1016/j.envpol.2021.117098

Liu, Q.; Sun, M.; Sun, X.; Liu, B.; Ostadhassan, M.; Huang, W.; Chen, X.; Pan, Z. 2023. Pore network characterization of shale reservoirs through state-of-the-art X-ray computed tomography: A review. In Gas Science and Engineering, 113, (2023), 204967. https://doi.org/10.1016/j.jgsce.2023.204967

Lüthi, M.; Bircher, B. A.; Meli, F.; Kung, A; Thalmann, R. 2019. X-ray flat-panel detector geometry correction to improve dimensional computed tomography measurements. Measurement Science and Technology, 31, (2020), 035002. https://doi.org/10.1088/1361-6501/ab52b1.

Mahdavi, M.; Mahvi, A. H.; Salehi, M.; Sadani, M.; Biglari, H.; Tashauoei, H. R.; Ebrahimi, A.; Yengejeh, R. J.; Fatehizadeh, A. 2020. Wastewater reuse from hemodialysis section by combination of coagulation and ultrafiltration processes: Case study in Saveh-Iran Hospital. Desalination and Water Treatment, 193, 274-283. https://doi.org/10.5004/dwt.2020.25799

Mahdavi, M.; Taheri, E.; Fatehizadeh, A.; Khiadani, M.; Hoseinzadeh, E.; Salehi, M.; Aminabhavi, T. M. 2024. Water recovery and treatment of spent filter backwash from drinking water using chemical reactor-ultrafiltration process. Journal of Water Process Engineering, 66, (2024), 105895. https://doi.org/10.1016/j.jwpe.2024.105895

Monga, R.; Deb, R.; Meyer, D. W.; Jenny, P. 2023. A probabilistic, flux-conservative particle-based framework for transport in fractured porous media. Advances in Water Resources, 172, (2023), 104368. https://doi.org/10.1016/j.advwatres.2023.104368.

Muzammil, M.; Zahid, A.; Farooq, U.; Saddique, N.; Breuer, L. 2023. Climate change adaptation strategies for sustainable water management in the Indus basin of Pakistan. Science of the Total Environment, 878, (2023), 163143. https://doi.org/10.1016/j.scitotenv.2023.163143

Nguyen, T. T.; Zhang, Z.; Wang, R.; Sawada, K.; Soda, S. 2024. Greywater treatment using lab-scale systems combining trickling filters and constructed wetlands with recycled foam glass and water spinach. Bioresource Technology Reports, 27, (2024), 101915. https://doi.org/10.1016/j.biteb.2024.101915

Nikon Metrology. 2015. X-Tek X-ray and CT Inspection CT Pro 3D for XT 6.10: User Manual XTM0977-A1. 82p.

Noutsopoulos, C.; Andreadakis, A.; Kouris, N.; Charchousi, D.; Mendrinou, P.; Galani, A.; Mantziaras, I.; Koumaki, E. 2018. Greywater characterization and loadings – Physicochemical treatment to promote onsite reuse. Journal of Environmental Management, 216, 337-346. https://doi.org/10.1016/j.jenvman.2017.05.094

Rouquerol, J.; Baron, G.; Denoyel, R.; Giesche, H.; Groen, J.; Klobes, P.; Levitz, P.; Neimark, A. V.; Rigby, S.; Skudas, R.; Sing, K.; Thommes, M.; Unger, K. 2012. Liquid intrusion and alternative methods for the characterization of macroporous materials (IUPAC technical report). Pure and Applied Chemistry, 84, 107-136. https://doi.org/10.1351/PAC-REP-10-11-19

Sacramento, R. N.; Yang, Y.; You, Z.; Waldmann, A.; Martins, A. L.; Vaz, A. S. L.; Zitha, P. L. J.; Bedrikovetsky, P. 2015. Deep bed and cake filtration of two-size particle suspension in porous media. Journal of Petroleum Science and Engineering, 126, 201-210. https://doi.org/10.1016/j.petrol.2014.12.001

Sadeghnejad, S.; Enzmann, F.; Kersten, M. 2022. Numerical Simulation of Particle Retention Mechanisms at the Sub-Pore Scale. Transport in Porous Media, 145, (1), 127-151. https://doi.org/10.1007/s11242-022-01843-y

Sakr, M.; El Agamawi, H.; Klammler, H.; Mohamed, M. M. 2023. A review on the use of permeable reactive barriers as an effective technique for groundwater remediation. In Groundwater for Sustainable Development, 21, (2023), 100914. https://doi.org/10.1016/j.gsd.2023.100914

Silva, M. T. Q. S.; Perretto, F.; do Rocio Cardoso, M.; Mazer, W. 2023. Porosity: Some characterization techniques. Materials Today: Proceedings. https://doi.org/10.1016/j.matpr.2023.03.716

Silvia, S.; Prasetya Aji, M.; Sustini, E.; Khairurrijal, K. 2012. Permeability, Strength and Filtration Performance for Uncoated and Titania-Coated Clay Wastewater Filters, 8, 79-94.

Song, J.; Huang, G.; Han, D.; Hou, Q.; Gan, L.; Zhang, M. 2021. A review of reactive media within permeable reactive barriers for the removal of heavy metal(loid)s in groundwater: Current status and future prospects. Journal of Cleaner Production, 319, (2021), 128644. https://doi.org/10.1016/j.jclepro.2021.128644

Song, S.; Le-Clech, P.; Shen, Y. 2023. Microscale fluid and particle dynamics in filtration processes in water treatment: A review. Water Research, 233, (2023), 119746. https://doi.org/10.1016/j.watres.2023.119746

Sun, J.; Dong, X.; Wang, J.; Schmitt, D. R.; Xu, C.; Mohammed, T.; Chen, D. 2016. Measurement of total porosity for gas shales by gas injection porosimetry (GIP) method. Fuel, 186, 694-707. https://doi.org/10.1016/j.fuel.2016.09.010

Tsekleves, E.; Cooper, R.; Spencer, J. 2021. Design for Global Challenges and Goals. Routledge, London, First Edition. 268p.

Volume Graphics GmbH. 2020. Reference Manual: VGSTUDIO MAX 3.4. 34p.

Wang, Y.; He, W.; Chen, C.; Zhang, X.; Tang, H.; Li, P.; Tong, Y.; Li, M.; Lin, Y.; Yu, J.; Xu, F.; Jia, X. 2022. Different countries need strengthen water management to improve human health. Journal of Cleaner Production, 380, (2022), 134998. https://doi.org/10.1016/j.jclepro.2022.134998

Warsame, A. A.; Abdi, A. H.; Amir, A. Y.; Azman-Saini, W. N. W. 2023. Towards sustainable environment in Somalia: The role of conflicts, urbanization, and globalization on environmental degradation and emissions. Journal of Cleaner Production, 406, (2023), 136856. https://doi.org/10.1016/j.jclepro.2023.136856

Wyczarska-Kokot, J.; Zabłocka-Godlewska, E.; Kudlek, E.; Lempart-Rapacewicz, A.; Pawlyta, M.; Marszałek, A. 2024. Multiparametric study of a filter bed from a swimming pool water treatment system. Desalination and Water Treatment, 319, (2024), 100579. https://doi.org/10.1016/j.dwt.2024.100579

Zu, X.; Li, Y.; Yin, B. 2023. Consecutive layer collaborative filter similarity for differentiable neural network pruning. Neurocomputing, 533, 35-45. https://doi.org/10.1016/j.neucom.2023.02.063